Size-Dependent Segregation Preference in Single-Atom Alloys of Late Transition Metals: Effects of Magnetism, Electron Correlation, and Geometrical Strain

Qiang Yin,[†,§] Fang Ma,[†,§] Yan Zhou,[†] Zhi-Jun Sui,[†] Xing-Gui Zhou,[†] De Chen,[‡] Yi-An Zhu[†,*]

[†]United Chemical Reaction Engineering Research Institute (UNILAB), State Key Laboratory of Chemical Engineering, East China University of Science and Technology, Shanghai 200237, China

[‡]Department of Chemical Engineering, Norwegian University of Science and Technology, N-7491 Trondheim, Norway

ABSTRACT: Dispersing isolated active metal atoms onto the surface of "inert" metal nanoparticles proves to be particularly effective in improving the catalytic performance of bimetallic catalysts. In this contribution, a quantity called average segregation energy (SE) is proposed to predict with reasonable accuracy the structural stability of single-atom alloy (SAA) clusters of late transition metals. By formulating an expression for this energy on the basis of Friedel's d-band model and under the tight-binding approximation, d-band filling is found to play a major role in determining the segregation behavior of all late transition metals. However, magnetism and electron correlation would greatly enhance the ability of 3d transition metals to segregate to the alloy surface, which can be explained by an improved model that includes both the two perturbations. Furthermore, by using the average SEs, the effect of geometrical strain is differentiated from the electronic and magnetic contributions, which, in contrast, may help to stabilize 3d transition metals in the core region by minimizing the lattice mismatch. Finally, we demonstrate that the size-dependent segregation preference has its origin in the size dependence of the electronic and structural properties of the SAA cluster.

1. Introduction

Singly dispersed metal atoms on solid supports such as metals, metal oxides, nanostructured carbon, etc.[1-2] have recently received much attention as novel catalysts for heterogeneous reactions. In particular, single-atom alloys (SAAs) whose electronic structures can be modified by changing the "inert" metals surrounding the active single-atom site exhibit adsorption and catalytic properties distinct from those of their constituent metals[3]. In some cases, however, the active single atoms may aggregate in the surface[4] or go into the sites beneath the outermost layer of the nanoparticle[5], leading to reduced specific activity. Hence, the key to the success of the SAAs in practical applications is to maintain the integrity of their unique chemical structures under various conditions.

It is generally accepted that in metal alloys the component that has a larger cohesive/surface energy tends to accumulate in bulk alloy to maximize metallic bonding and the component with a larger atomic radius prefers to stay on the surface to relieve compressive strain[6]. Although these generalizations are valid under most circumstances, such empirical observations cannot help us to make a reasonably reliable prediction about the segregation preference in a particular binary alloy. Furthermore, in light of this information, one cannot understand the physical origin of surface segregation without successfully separating the contributions from different electronic and structural properties of nanoparticles.

Traditionally, the surface segregation energy (SE) is a measure of the energy change associated with moving an impurity metal atom from the core to the shell of a bimetallic cluster, which is routinely used to predict whether the minority active elements would accumulate on the surface of the inert host to form a thermodynamically stable structure[7-8]. The pioneering work by Ruban et al. presented a database of 24 × 24 SEs of transition metals in both close-packed[9] and open surfaces[10] by using the GF-LMTO method. More recently, Wang et al.[11] systematically calculated the SEs of late transition metals by the DFT-GGA method and employing a cuboctahedral cluster model of 55 atoms. Comparison of the results from the two groups shows that, the predicted core-to-shell sequence of transition metals resemble each other but the numerical agreement is in fact quite poor, and, more importantly, there are some conflicting predictions about the sign of the SEs. One example is the PtCu bimetallic cluster, which was found to adopt a Pt-shell/Cu-core structure if the surface was dominated by close-packed arrays of atoms. However, when the metal particle became smaller and was surrounded by under-coordinated sites, as in the case of the 55 atom cuboctahedral cluster,

a reverse segregation was predicted, no matter which component served as the impurity. Since it was reported experimentally that the ordering of atoms in bimetallic nanoparticles may vary with their particle size[12-14], the discrepancy between the two sets of data is probably due to the size dependence of the structural stability of the SAAs.

Another problem with the determination of the segregation preference in SAAs by using the tabulated segregation energies is the difficulty of memorizing their magnitudes and signs all. Even if the needed values are sometimes at hand, we can get lost in the details if we don't see the general patterns. Thus, recognizing a pattern of the segregation energies for a

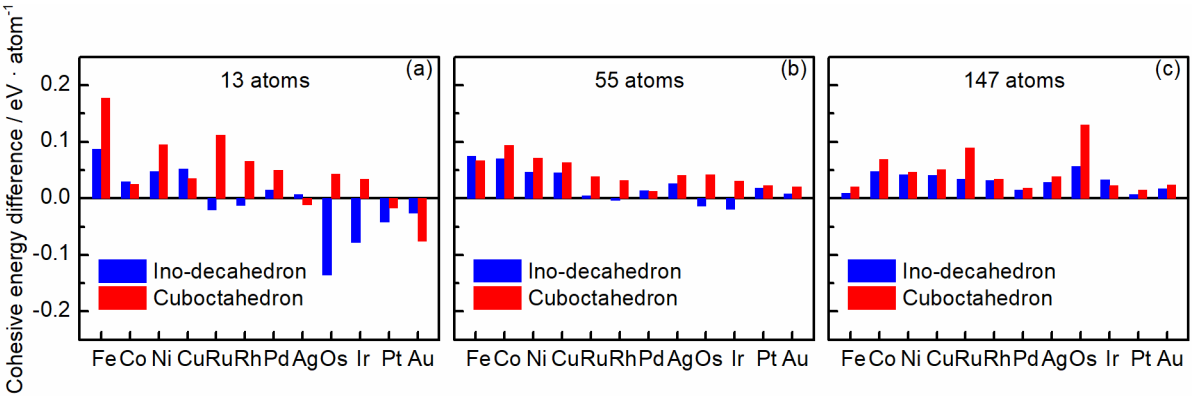

Figure 1. Calculated cohesive energy differences of cuboctahedral and decahedral clusters from their icosahedral counterparts at different particle sizes.

class of binary combinations of transition metals not only can free us from learning (or trying to memorize) many individual facts but also would give us a broader understanding of the key factors that influence the core-to-shell sequence. Inspired by "the activity series" that can be used to predict whether a certain metal will be oxidized by the ion of another metal, we suggest in this work that a quantity called averaged SE can be used to provide a direct measure of the segregation preference in SAA clusters of late transition metals. Icosahedral SAA clusters of 13, 55, and 147 atoms of 12 late transition metals from group 8B to group 1B are first constructed and the SE of single impurities in their binary combinations is calculated by using the DFT method. The reason the late transition metals have been the focus of much research is that they are among the most widely used heterogeneous catalysts in a number of chemical and biochemical applications. Then, the effects of magnetism, electron correlation, and geometrical strain on the segregation trend is explored by formulating an expression for the average SE on the basis of Friedel's d-band model and under the tight-binding approximation. Finally, we conclude by discussing the implication of our results for understanding the origin of the size-dependent segregation preference in SAAs.

2. Computational details

2.1 Model construction

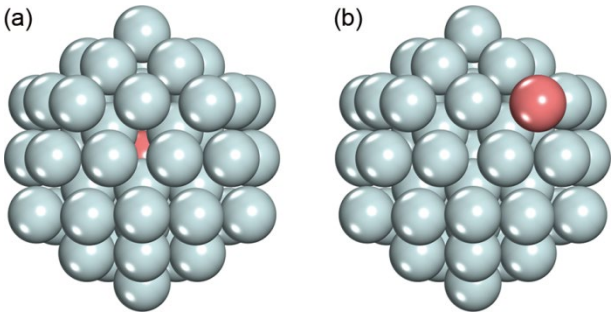

Figure 2. Illustrations of icosahedral clusters of 55 atoms with an impurity (a) at the center of the core and (b) at the corner of the shell.

To construct a reasonable description of nanometer-sized clusters, we first examined the structural, energetic, and magnetic properties of 12 late-transition-metal nanoparticles of 13, 55, and 147 atoms by the DFT method, where the three highly symmetrical structural motifs (cuboctahedron, Ino decahedron, and icosahedron) are taken into consideration (see Figure S1). It is generally accepted that icosahedral clusters are energetically favorable at small sizes while truncated octahedron is the preferred geometry of large metal particles, and in between truncated decahedra dominate[15-16]. This observed trend is a result of two competing forces. On the one hand, quasi-spherical shape and close-packed surface would effectively decrease the surface energy of small metal clusters. On the other hand, the internal strain in bulk metal proves to be the dominant factor in influencing the structural stability of large particles and crystalline structures are thus strongly favored.

Figure 1 shows the calculated cohesive energy differences of the cuboctahedral and decahedral clusters from

their icosahedral counterparts at different particle sizes. The more positive the values, the energetically less stable are the former two structural motifs. One can see from the figure that there exists a thermodynamic preference for the late-transition-metal nanoparticles to adopt the icosahedral geometry at the particle sizes under consideration. Previously, Baletto et al.[17] compared the structural stability of the different motifs by performing semi-empirical calculations and found the nanoparticles undergo a transition from icosahedron to the fcc fashion at a crossover size of ~500 atoms, which provided evidence in support of our predication about the energetically favorable conformation. On the other hand, according to Ferrando et al.[18-23], the central site of icosahedron is strongly compressed compared to crystalline structures, which would destabilize the system to some extent. It is therefore important to note that, although icosahedron does not necessarily correspond to the global minimum of the potential energy surface constructed as a given nanoparticle evolves, calculations carried out on this specific motif would not change the way in which the electronic and magnetic properties influence the segregation trend in SAAs. Moreover, as we will see in Sec. IIIC, this compression offers an opportunity for examining the strain effect on the segregation behavior of impurities of different atomic sizes. Hence, icosahedron is applied in this work to represent the geometrical and electronic structures of late-transition-metal alloys.

2.2 DFT calculation

All DFT calculations were carried out using the Vienna Atomic Simulation Package (VASP)[24]. The exchange and correlation in the Kohn-Sham theory was treated with the generalized gradient approximation in the form of the PBE functional[25]. The projector-augmented wave (PAW) method[26-27] was used to describe the electron-ion interaction and for the

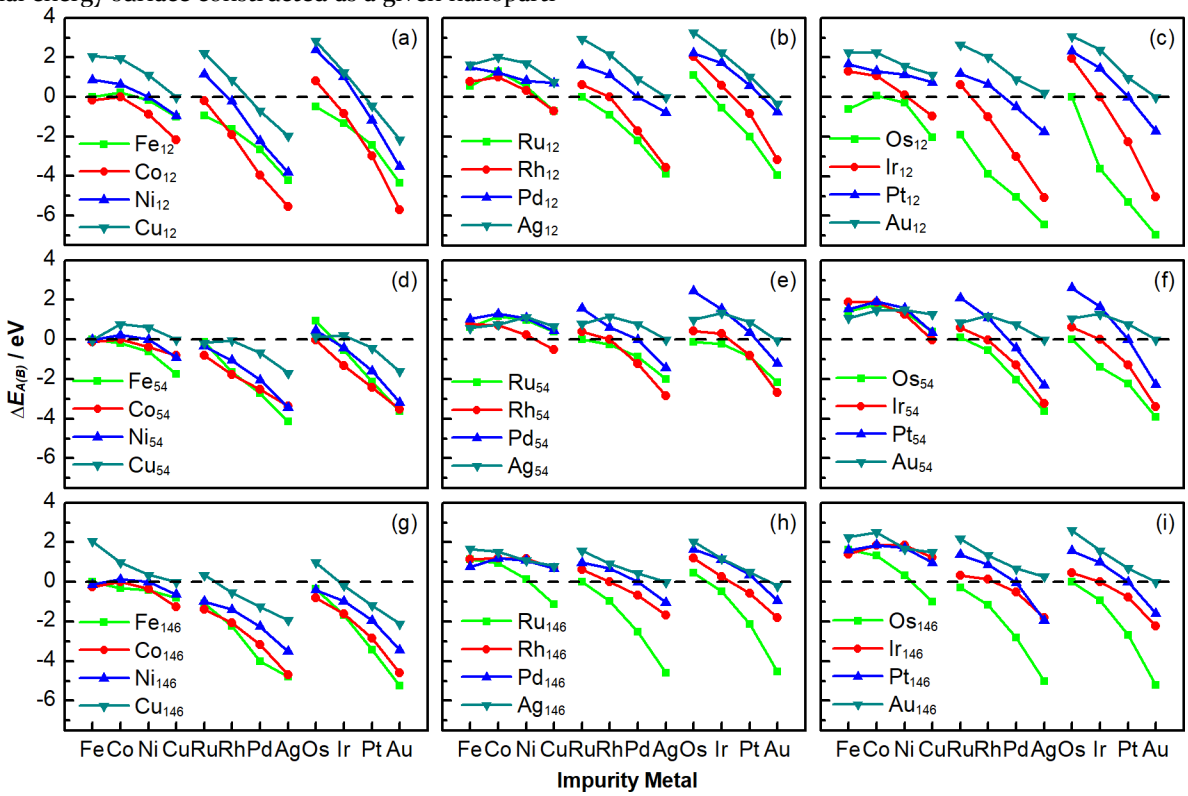

Figure 3. Segregation energies in 13, 55, and 147 atom icosahedral SAA clusters. The negative (positive) value indicates the impurity metal is more likely to segregate to the shell (core) of the host.

plane wave basis set a kinetic energy cutoff of 400 eV was applied to converge the total energy per atom to within 1 meV. The Gaussian smearing method with an energy smearing of 0.05 eV was used to determine the partial occupancies of the orbitals (or bands). It has long been recognized that the magnetism of nanostructured materials are greatly enhanced compared to their bulk counterparts. The reduced dimensions, the reduced coordination of atoms on the surface, and the quantum mechanical effects at the nanoscale dimensions not only gives rise to larger magnetic moments per atom in conventional magnetic materials but also results in the superparamagnetism of otherwise nonmagnetic materials[28-29]. Hence, spin-polarized calculations were performed unless otherwise specified, in which ferromagnetic ordering was adopted. The results shown in Figure S3 supports the idea that inclusion of the magnetism effect is of vital importance for obtaining reasonably accurate structures and energetics of nanoparticles.

All transition-metal atoms in the clusters were allowed to relax in a box with dimensions of 20 Å × 20.5 Å × 21 Å. The Monkhorst-Pack scheme was used to sample the irreducible part of the first Brillouin zone and for the isolated nanoparticles only the Gamma-point was required. Geometry optimization was considered to be converged when the forces on each atom were better than 0.03 eV/Å.

3. Results and discussion

3.1 Trend in the surface segregation energy

The surface segregation energy in SAAs was calculated as the energy difference of the clusters (see Figure 2) with the impurity (A) in the core and on the shell of the host (B):

$$\Delta E_{A(B)} = E^{shell}_{A(B)} - E^{core}_{A(B)} \quad (1)$$

Under this definition, the impurity metal tends to stay on the surface of the host metal if the surface segregation energy is negative; the greater the magnitude, the greater is the tendency. The use of the same structural motif and segregation sites ensures that local geometry of nanoparticles and coordination environment of atoms have no effect on the trend in the calculated values (see Sec. S5 for details).

It can be seen from Figure 3 that for a given host the SE of the impurities generally becomes more negative as we move from left to right in each row of the periodic table, indicating an increased ability to segregate to the surface of the host. Not surprisingly, nearly the same ordering is observed when comparing the SEs of a specific impurity metal in a series of hosts that are within the same period. Exceptions to the general trend may occur if the 3*d* transition metals are alloyed with other elements. For example, the SEs of the 3*d* transition metals in Rh_{12} vary in the order $Rh_{12}Cu < Rh_{12}Ni < Rh_{12}Fe < Rh_{12}Co$.

In textbooks of physics and chemistry, a list of metals arranged in order of decreasing the ease of oxidation can often be found, which is called the activity series and can be used to predict the outcome of reactions between metals and either metal salts or acids. Any metal on the list can be oxidized by the ions of elements below (or behind) it. Thus, the questions that could be of practical importance as well as chemical interest are whether there exists a general core-to-shell sequence if late transition metals from different periods are considered altogether and how this sequence, if any, varies with the particle size.

3.2 Average segregation energy

The simplest way of predicting the segregation trend in binary combinations is to compare the SEs of various impurity metals in a given host. By varying the host, however, the resulting trends could be slightly different (see Figure 3), which is due to the unique features of certain combinations that arise from specific interactions between their constituent atoms. If we could minimize the disturbing influence of these interactions, then the relative abilities of impurity metals to segregate to the cluster surface can be probed.

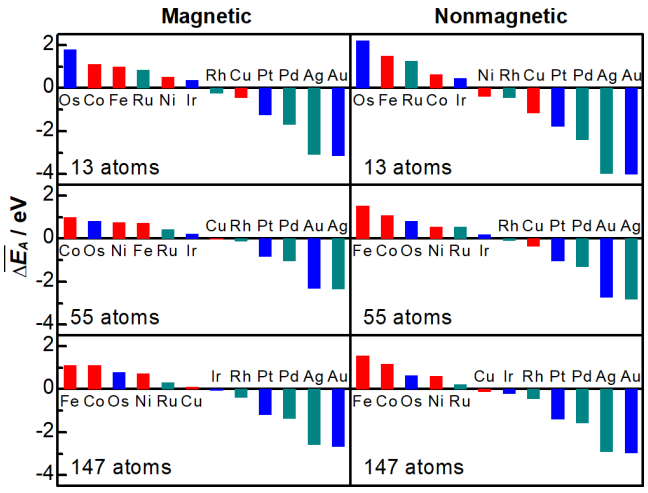

Figure 4. Average SEs of late transition metals in magnetic and nonmagnetic icosahedral SAA clusters of 13, 55, and 147 atoms.

Hence, we bring in the notion of average SE to quantitatively measure the ability of a particular late transition metal to stay on the surface of alloys, which is defined as the mean value of the SEs of this impurity in the host of other late transition metals:

$$\overline{\Delta E_A} = \frac{1}{12}\sum_{B=Fe}^{Au} \Delta E_{A(B)} \quad (2)$$

In this way, the two-dimensional databases of SEs that are commonly encountered in the previous studies[9, 11] can be transformed into a one-dimensional list. It should be noted that, although the numerical value of the average SEs is strongly dependent on the chosen metal set, their relative magnitudes provide an adequate and useful description of the segregation preference in the SAAs composed of the metals in the data set. In Figure 4, the transition metals are arranged in order of increasing ease of accumulation in the shell region of bimetallic clusters; that is, any metal on the list tends to segregate to the surface of the metals on its left. For example, Pd is on the right of Cu in the six series regardless of the particle size and magnetic state. We therefore expect Pd to stay on the shell of the Pd-Cu alloy. Indeed, there is experimental evidence from high-resolution scanning tunneling microscopy (STM) images that isolated Pd atoms can be stabilized on the PdCu SAA catalysts[30]. Furthermore, it follows from the definition of the average SE that this quantity can be used to compare the stabilities of different combinations of late transition metals; the greater the difference in the average SE between the two components, the energetically more favorable is the resulting SAA cluster.

It is important to note that although arranging the late transition metals by average SE may lead to different orders at different particle sizes and in different magnetic states, there do exist some general trends: 1) the average SEs of the 4*d* and 5*d* transition metals exhibit nearly the same pattern in all the six series, namely, Os > Ru > Ir > Rh > Pt > Pd > Au ≈ Ag, corresponding to their positions in the periodic table first by group from left to right and then by period from bottom to top; 2) although the core-

to-shell sequence of the magnetic 3*d* transition metals varies greatly with the cluster size, their average SEs in the nonmagnetic state follow the same order Fe > Co > Ni > Cu, which means the magnetic property plays a key role in determining the core-shell preference of the magnetic metals; 3) as the cluster size increases, the discrepancy between the sequences obtained by the spin-polarized and non-spin-polarized calculations becomes smaller and even the same sequence can be found at the particle size of ~1.5 nm (147 atoms). It can therefore be deduced that the magnetic property of the 3*d* late transition metals has a great influence on their segregation preference in small clusters and the influence declines gradually as the cluster size is increased.

Figure 5 illustrates the color-coded matrices that are created by using the SE data given in Figure 3, with the late transition metals arranged in order of decreasing average SE. In the matrices, the SE becomes more negative as we proceed toward the upper right, and the closer to the lower left corner, the more readily will the impurity go into the core region. Compared with the matrices where the elements are ordered in terms of atomic number (see Figure S5), the matrices in Figure 5 show clearly a blue-to-red gradient, indicating the average SE is of extraordinary power in predicting whether a certain metal will segregate to the surface when alloyed with other metals at a particular particle size.

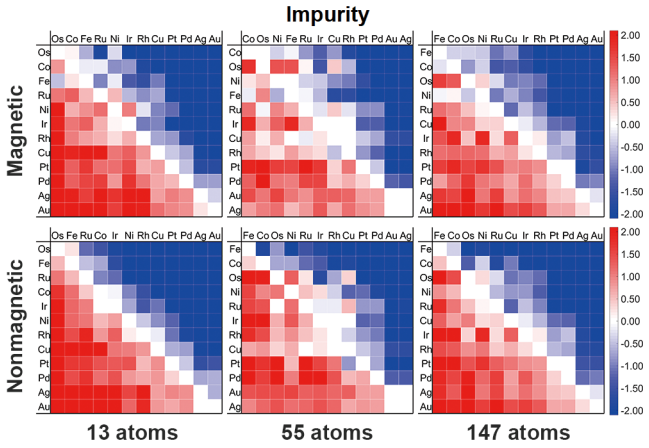

Figure 5. Color-coded matrix of segregation energies for 13, 55, and 147 atom clusters. The blue (red) square indicates that the impurity atom tends to be in the shell (core) when alloyed with the host metal.

3.3 Origin of size-dependent segregation trend

To gain further insight into the size dependence of the segregation trend in SAAs and explain the origin of the different segregation behaviors of the 3*d* and 4,5*d* transition metals, it is advantageous to refer to Friedel's *d*-band model [31], which has been successfully used to understand the variation in the cohesive energy and alloy formation heat of transition metals in terms of *d*-band bonding. In the context of this model, the *d*-band energy of a transition-metal atom is determined by the *d*-band width and *d*-band filling. Under the tight-binding approximation[32], the *d*-band width is proportional to the square root of the effective coordination number of the transition-metal atom. Hence, if we assume to a first approximation that the surface-core level shift of any transition metal equals its *d*-band energy change accompanying the migration of the atom from the core to the shell of a cluster[33], the SE in SAAs can be written as (A derivation of this equation is given in Sec. S6)

$$\Delta E_{A(B)} = -5W_{core,B}\cdot\left(\sqrt{\frac{Z_{shell}}{Z_{core}}}-1\right)\cdot\left(\mu_{d,A}-\mu_{d,B}\right) \qquad (3)$$

where $W_{core,B}$ is the effective *d*-band width of the host atom in the core of the cluster and would vary with the particle size, Z_{shell} and Z_{core} are the effective coordination number of the atom on the shell and in the core, respectively, and μ_d is a quantity characterizing the interaction between the d electrons in the constituent metals, which is defined as $\mu_d = \frac{N_d}{10}\left(1-\frac{N_d}{10}\right)$ and can be calculated from the value of *d*-band filling (N_d) summarized in Harrison's solid-state table[34].

Then we extend the arguments to the average SE. Combining Equation 1 and Equation 2 gives

$$\overline{\Delta E_A} = -5\overline{W_{core,B}}\cdot\left(\sqrt{\frac{Z_{shell}}{Z_{core}}}-1\right)\cdot\mu_{d,A}-\overline{\Delta E_{d,B}^{core\to shell}} \qquad (4)$$

where $\overline{\Delta E_{d,B}^{core\to shell}}$ is the average value of $-5W_{core,B}\left(\sqrt{\frac{Z_{shell}}{Z_{core}}}-1\right)\mu_{d,B}$ and $\overline{W_{core,B}}$ is the average value of $W_{core,B}$ for all the binary alloys of the impurity A, both of which remain constant regardless of the chemical identity of the impurity metal. Hence, according to the equation, the variation of the average SE is determined by the change in $\mu_{d,A}$ and there should be a linear scaling relation between these two quantities. More importantly, only in this way can the ability of the impurity metal A to segregate to the cluster surface be correlated solely with its intrinsic property, which in turn helps to identify the key factors that influence the size-dependent segregation trend.

3.3.1 Effect of magnetism and electron correlation

Figure 6a-f shows the average SEs of the late transition metals in the icosahedral SAA clusters as a function of $\mu_{d,A}$ (The average SEs are also plotted against the surface energies of close-packed surfaces in Figure S11 for comparison). Indeed, the plots for the 4*d* and 5*d* transition metals show straight lines regardless of the particle size and magnetic state. The positive slope of the straight lines means that the segregation of impurity metals to the surface becomes energetically less favorable as the value of $\mu_{d,A}$ rises. In other words, the *d*-band filling plays a major role in determining the segregation preference of the 4*d* and 5*d* transition metals. On the other hand, the least-squares fitted lines for the alloys in the nonmagnetic state are slightly steeper than those in the magnetic state,

which implies that magnetism has a minor but negative effect on the segregation of the combinations of the 4*d* and 5*d* transition metals.

As for the 3*d* transition metals, the dependence of the average SE on the $\mu_{d,A}$ exhibits a distinctly different pattern. In particular, the fitted lines for the magnetic results, especially at the upper end, are curved downward compared to those for the 3*d* transition metals in the nonmagnetic state, which indicates that the tendency for the 3*d* transition metals to stay on the alloy surfaces is enhanced by the electron spin magnetism and the influence becomes greater with decreasing the *d*-band filling. On the other hand, although the nonmagnetic results give good straight lines, the resulting scaling relations lie above those for the 4*d* and 5*d* metals, with a much smaller slope. Hence, some factor other than the magnetic property must be at work in determining the segregation preference of the 3*d* transition metals.

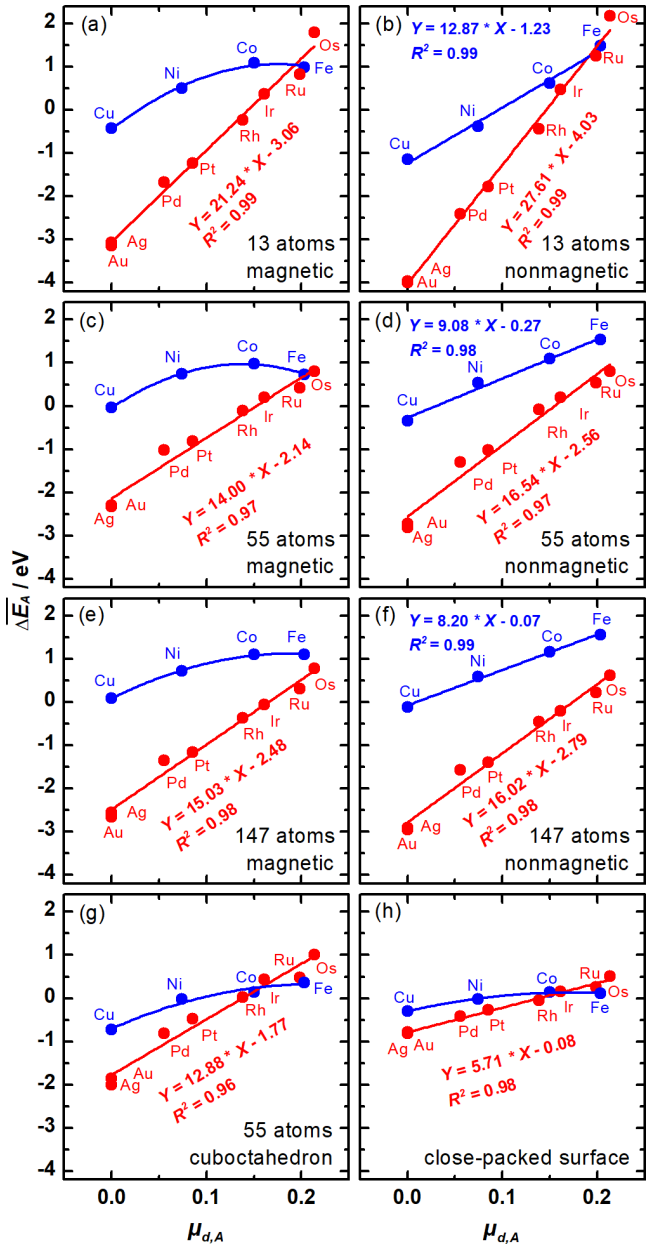

Figure 6. Plots of the average SE of late transition metals as a function of $\mu_{d,A}$ in 13, 55, and 147 atom icosahedral clusters in the magnetic (a, c, and e) and nonmagnetic (b, d, and f) state. The data for (g) 55 atom cuboctahedral clusters and (h) close-packed surfaces are also presented for comparison.

To explain the variation in the cohesive energy of the 3*d* transition metals, Friedel and Harrison refined the rectangular *d*-band model by including the contributions from magnetism and *d* electron correlation as perturbations[35-36]. In much the same way, Equation 4 can be extended to a more general one:

$$\overline{\Delta E_A} = -5\left(\overline{\sqrt{W_{core,B}^2+U_A^2}}-U_A\right)\cdot\left(\sqrt{\frac{Z_{shell}}{Z_{core}}}-1\right)\cdot\mu_{d,A} - \overline{\Delta E_{d,B}^{core\rightarrow shell}}+\overline{\Delta E_A^{mag}} \quad (5)$$

where

$$\Delta E_A^{mag} = \left(U_A+4J_A-W_{core,A}\right)\frac{M_{core,A}^2}{20} - \left(U_A+4J_A-W_{shell,A}\right)\frac{M_{shell,A}^2}{20} \quad (6)$$

where U_A and J_A are the intra-atomic Coulomb and exchange interactions of the impurity A, respectively, and M_A is the magnetic moment. Because the band width and magnetic moment are known to decrease and increase, respectively, as the impurity migrates from the core to the shell of the cluster, it follows that the ΔE_A^{mag} takes a negative value and causes the 3*d* metals to show more preference for the alloy surface than expected.

In addition to the magnetic property, electron correlation is of crucial importance in determining the ground-state properties of the 3*d* transition metals which have a narrow band width compared to the 4*d* and 5*d* metals. As seen in Figure 6, the slope of the $\overline{\Delta E_A}$ vs. $\mu_{d,A}$ plot for the 3*d* metals in the nonmagnetic state is far less steep than that for the 4*d* and 5*d* metals. This deviation can be traced to the strong Coulomb correlation between the electrons as a result of the relatively weak spatial extension of the 3*d* orbitals[37]. The reasoning behind this remark is that the U_A value is no longer negligibly small and would give a less positive value of the $\sqrt{W_{core,B}^2+U_A^2}-U_A$ term in Equation 5.

3.3.2 Effect of geometrical strain

Although the improved Friedel model can successfully explain the deviation of the $\overline{\Delta E_A}$ vs. $\mu_{d,A}$ plot for the 3*d* metals from a straight line, it is still not clear why the fitted line lies above that for the 4,5*d* metals. As discussed in Sec. IIA, the central site of icosahedron is strongly compressed, and it is therefore rational to expect that the occupation of this site by an impurity of a large atomic size compared to the host may give rise to great geometrical strain, thereby incurring high energy cost.

Because the Wigner-Seitz radius of the 3*d* metals is much smaller than that of the 4*d* and 5*d* metals[38] (see Fig-

ure S13), it is energetically unfavorable for the 4,5*d* metals to stay in the core region of icosahedral clusters of 3*d* metals. As a consequence, the average SEs of the 4*d* and 5*d* metals lie on the same straight line, but the data for the 3*d* metals shift towards a more positive value. The separation between the two fitted lines naturally defines the geometrical strain effect and can therefore differentiate this effect from the electronic and magnetic contributions.

Then we examine if the predicted segregation trend holds true when clusters with other geometries or extended surfaces are concerned. The previously published SEs of late transition metals in 55 atom fcc cuboctahedra[11] and close-packed surfaces[9] are reconstructed and presented in Figure 6g and 6h, respectively, for comparison. One can see that the shape of the average SE curves closely resemble those reported in the present work, although the figures differ somewhat in the relative locations of the curves. The reason for the reduced separation between the two fitted lines is that there is less geometrical distortion and lattice contraction in the crystalline structures and, consequently, the energy cost arising from the aforementioned lattice mismatch at the core region of the host 3*d* metals is much lower than that for icosahedron. In particular, the comparison between the results at the same particle size (see Figure 6c and 6g) provides direct evidence in support of the idea that the segregation preference depends strongly upon crystal structure and geometrical strain[9].

3.3.3 Size dependence of segregation preference

The last and most important information given by Figure 6 is that the cluster size has a major impact on the dependence of the $\overline{\Delta E_A}$ upon the *d*-band filling. First, if we compare our calculated results to that for the close-packed surfaces, it is interesting to find that the $\overline{\Delta E_A}$ of the 4*d* and 5*d* impurity metals becomes less sensitive to the *d*-band filling as the particle size is raised, resulting from the increased effective coordination number of the shell atoms (Z_{shell} in Equation 4). As a consequence, the tendency for alloys to segregate is lowered.

Second, the plots for the magnetic 3*d* transition metals become less curved as the cluster size rises, which is due to the high magnetic moments in the small clusters that would greatly enhance the effect of magnetism on the segregation preference.

Third, the difference in the slope of the linear scaling relations between the 3*d* and 4,5*d* metals in the nonmagnetic state gradually decreases as we move from the 13 through 55 and eventually to 147 atom clusters, signifying a weakened influence of electron correlation and hence an enhanced preference of the 3*d* metals for the core region.

Finally, the separation between the $\overline{\Delta E_A}$ vs. $\mu_{d,A}$ plots for the 3*d* and 4,5*d* metals is decreased either as the particle size of icosahedra increases from ~0.5 nm to ~1.5 nm or when moving from the fcc cuboctahedra to the close-packed surfaces. It was reported that, for icosahedra of less than 147 atoms and cuboctahedra, their excess energy with respect to a bulk solid becomes less positive as the Ag nanoparticle size increases[21]. Hence, the approaching of the two fitted lines, which is indicative of a weaker tendency for the 3*d* metals to stay in the core region, is a consequence of the decrease in the volume strain in clusters with increasing particle size (which is valid for both icosahedra of less than 147 atoms and cuboctahedra).

4. Conclusion

To summarize, we have identified the average SE of late transition metals as a good measure of the segregation preference in sing-atom alloy (SAA) clusters. An expression is formulated for this quantity on the basis of Friedel's *d*-band model and under the tight-binding approximation. The calculated results indicate the *d*-band filling plays a major role in determining the segregation preference of the 4*d* and 5*d* transition metals. In an improved model that includes the contributions of magnetism and electron correlation, the physical origin of the different segregation behaviors of the 3*d* and 4,5*d* transition metals is explained. It turns out that both of these two contributions may enhance the ability of the 3*d* transition metals to segregate toward the surface. Furthermore, by using the average SEs, the geometrical strain effect that is not included in the Friedel model can be differentiated from the electronic and magnetic contributions, which is found to play a beneficial role in stabilizing the 3*d* metals in the core region. As the particle size rises, the increased effective coordination number of the shell atoms and the weakened influences of magnetism, electron correlation, and geometrical strain may give rise to a lowered tendency for alloys to segregate. Our theoretical model offers an explanation for the size-dependent segregation preference in SAA clusters and may serve as a guideline for rational design of stable SAA catalysts and nanoplasmonic dimers[39].

ASSOCIATED CONTENT

Supporting Information.
Comparison of geometries and energetics of three structural motifs; size-dependent properties of 12 late-transition-metal clusters; segregation energies and electronic structures of icosahedral single-atom alloy clusters; effect of segregation site on segregation preference; derivation of the relationship between segregation energy and d-band filling of transition metals; correlation between average segregation energy and surface energy; Effect of magnetism on segregation energy; Wigner-Seitz radius of 12 late transition metals. This material is available free of charge via the Internet at http://pubs.acs.org.

AUTHOR INFORMATION

Corresponding Author

*Email: yanzhu@ecust.edu.cn

Notes

The authors declare no competing financial interest.
§ These authors contributed equally to this work.

ACKNOWLEDGMENT

This work is supported by the Natural Science Foundation of China (91645122, 21473053, and U1663221), the National Key Research and Development Program of China (2018YFB0604700), and the Fundamental Research Funds for the Central Universities (2222017l8003).

REFERENCES

1. Yang, X.-F.; Wang, A.; Qiao, B.; Li, J.; Liu, J.; Zhang, T., Single-Atom Catalysts: A New Frontier in Heterogeneous Catalysis. *Acc. Chem. Res.* **2013**, *46*, 1740-1748.
2. Yan, H.; Cheng, H.; Yi, H.; Lin, Y.; Yao, T.; Wang, C.; Li, J.; Wei, S.; Lu, J., Single-Atom Pd_1/Graphene Catalyst Achieved by Atomic Layer Deposition: Remarkable Performance in Selective Hydrogenation of 1,3-Butadiene. *J. Am. Chem. Soc.* **2015**, *137*, 10484-10487.
3. Darby, M. T.; Réocreux, R.; Sykes, E. C. H.; Michaelides, A.; Stamatakis, M., Elucidating the Stability and Reactivity of Surface Intermediates on Single-Atom Alloy Catalysts. *ACS Catal.* **2018**, *8*, 5038-5050.
4. Campbell, C. T., The Energetics of Supported Metal Nanoparticles: Relationships to Sintering Rates and Catalytic Activity. *Acc. Chem. Res.* **2013**, *46*, 1712-1719.
5. Lucci, F. R.; Lawton, T. J.; Pronschinske, A.; Sykes, E. C. H., Atomic Scale Surface Structure of Pt/Cu(111) Surface Alloys. *J. Phys. Chem. C* **2014**, *118*, 3015-3022.
6. Ferrando, R.; Jellinek, J.; Johnston, R. L., Nanoalloys: From Theory to Applications of Alloy Clusters and Nanoparticles. *Chem. Rev.* **2008**, *108*, 845-910.
7. Greeley, J.; Mavrikakis, M., Alloy Catalysts Designed from First Principles. *Nat. Mater.* **2004**, *3*, 810-815.
8. Kyriakou, G.; Boucher, M. B.; Jewell, A. D.; Lewis, E. A.; Lawton, T. J.; Baber, A. E.; Tierney, H. L.; Flytzani-Stephanopoulos, M.; Sykes, E. C. H., Isolated Metal Atom Geometries as a Strategy for Selective Heterogeneous Hydrogenations. *Science* **2012**, *335*, 1209-1212.
9. Ruban, A. V.; Skriver, H. L.; Norskov, J. K., Surface Segregation Energies in Transition-Metal Alloys. *Phys. Rev. B* **1999**, *59*, 15990-16000.
10. Nilekar, A. U.; Ruban, A. V.; Mavrikakis, M., Surface Segregation Energies in Low-Index Open Surfaces of Bimetallic Transition Metal Alloys. *Surf. Sci.* **2009**, *603*, 91-96.
11. Wang, L. L.; Johnson, D. D., Predicted Trends of Core-Shell Preferences for 132 Late Transition-Metal Binary-Alloy Nanoparticles. *J. Am. Chem. Soc.* **2009**, *131*, 14023-14029.
12. Oezaslan, M.; Heggen, M.; Strasser, P., Size-Dependent Morphology of Dealloyed Bimetallic Catalysts: Linking the Nano to the Macro Scale. *J. Am. Chem. Soc.* **2012**, *134*, 514-524.
13. Rong, C. B.; Li, D.; Nandwana, V.; Poudyal, N.; Ding, Y.; Wang, Z. L.; Zeng, H.; Liu, J. P., Size-Dependent Chemical and Magnetic Ordering in $L1_0$-Fept Nanoparticles. *Adv. Mater.* **2006**, *18*, 2984-2988.
14. Froemming, N. S.; Henkelman, G., Optimizing Core-Shell Nanoparticle Catalysts with a Genetic Algorithm. *J. Chem. Phys.* **2009**, *131*, 234103.
15. Baletto, F.; Ferrando, R., Structural Properties of Nanoclusters: Energetic, Thermodynamic, and Kinetic Effects. *Rev. Mod. Phys.* **2005**, *77*, 371-423.
16. Logsdail, A. J.; Paz-Borbon, L. O.; Downing, C. A., Dft-Computed Trends in the Properties of Bimetallic Precious Metal Nanoparticles with Core@Shell Segregation. *J. Phys. Chem. C* **2018**, *122*, 5721-5730.
17. Baletto, F.; Ferrando, R.; Fortunelli, A.; Montalenti, F.; Mottet, C., Crossover among Structural Motifs in Transition and Noble-Metal Clusters. *J. Chem. Phys.* **2002**, *116*, 3856-3863.
18. Mottet, C.; Rossi, G.; Baletto, F.; Ferrando, R., Single Impurity Effect on the Melting of Nanoclusters. *Phys. Rev. Lett.* **2005**, *95*, 035501.
19. Bochicchio, D.; Ferrando, R., Morphological Instability of Core-Shell Metallic Nanoparticles. *Phys. Rev. B* **2013**, *87*, 165435.
20. Panizon, E.; Bochicchio, D.; Rossi, G.; Ferrando, R., Tuning the Structure of Nanoparticles by Small Concentrations of Impurities. *Chem. Mater.* **2014**, *26*, 3354-3356.
21. Ferrando, R., *Structure and Properties of Nanoalloys*; Elsevier: Amsterdam, 2016; Vol. 10.
22. Panizon, E.; Ferrando, R., Strain-Induced Restructuring of the Surface in Core@Shell Nanoalloys. *Nanoscale* **2016**, *8*, 15911-15919.
23. Palomares-Baez, J. P.; Panizon, E.; Ferrando, R., Nanoscale Effects on Phase Separation. *Nano Lett.* **2017**, *17*, 5394-5401.
24. Kresse, G.; Furthmüller, J., Efficiency of Ab-Initio Total Energy Calculations for Metals and Semiconductors Using a Plane-Wave Basis Set. *Comp. Mater. Sci.* **1996**, *6*, 15-50.
25. Perdew, J. P.; Burke, K.; Ernzerhof, M., Generalized Gradient Approximation Made Simple. *Phys. Rev. Lett.* **1996**, *77*, 3865-3868.
26. Blöchl, P. E., Projector Augmented-Wave Method. *Phys. Rev. B* **1994**, *50*, 17953-17979.
27. Kresse, G.; Joubert, D., From Ultrasoft Pseudopotentials to the Projector Augmented-Wave Method. *Phys. Rev. B* **1999**, *59*, 1758.
28. Singh, R., Unexpected Magnetism in Nanomaterials. *J. Magn. Magn. Mater.* **2013**, *346*, 58-73.
29. Bader, S. D., Colloquium: Opportunities in Nanomagnetism. *Rev. Mod. Phys.* **2006**, *78*, 1.
30. Boucher, M. B.; Zugic, B.; Cladaras, G.; Kammert, J.; Marcinkowski, M. D.; Lawton, T. J.; Sykes, E. C.; Flytzani-Stephanopoulos, M., Single Atom Alloy Surface Analogs in $Pd_{0.18}Cu_{15}$ Nanoparticles for Selective Hydrogenation Reactions. *Phys. Chem. Chem. Phys.* **2013**, *15*, 12187-12196.
31. Friedel, J., *The Physics of Metals*; Cambridge University Press: New York, 1971; Vol. 1.
32. Andersen, O. K.; Jepsen, O., Explicit, First-Principles Tight-Binding Theory. *Phys. Rev. Lett.* **1984**, *53*, 2571-2574.
33. Aldén, M.; Abrikosov, I. A.; Johansson, B.; Rosengaard, N. M.; Skriver, H. L., Self-Consistent Green's-Function Technique for Bulk and Surface Impurity Calculations: Surface Core-Level Shifts by Complete Screening. *Phys. Rev. B* **1994**, *50*, 5131-5146.
34. Harrison, W. A., *Electronic Structure and the Properties of Solids: The Physics of the Chemical Bond*; Dover Publications: New York, 1989.
35. Friedel, J.; Sayers, C. M., On the Role of D-D Electron Correlations in the Cohesion and Ferromagnetism of Transition Metals. *J. Phys. France* **1977**, *38*, 697-705.
36. Harrison, W. A., *Theoretical Alchemy: Modeling Matter*; World Scientific: Singapore, 2010.
37. Martins, C.; Aichhorn, M.; Biermann, S., Coulomb Correlations in 4d and 5d Oxides from First Principles or How Spin-Orbit Materials Choose Their Effective Orbital Degeneracies. *J. Phys.: Condens. Matter* **2017**, *29*, 263001.
38. Kittel, C.; McEuen, P., *Introduction to Solid State Physics*, 8th ed.; John Wiley & Sons: New Delhi, 2015.
39. Downing, C. A.; Mariani, E.; Weick, G., Radiative Frequency Shifts in Nanoplasmonic Dimers. *Phys. Rev. B* **2017**, *96*, 155421.

TOC Graphic

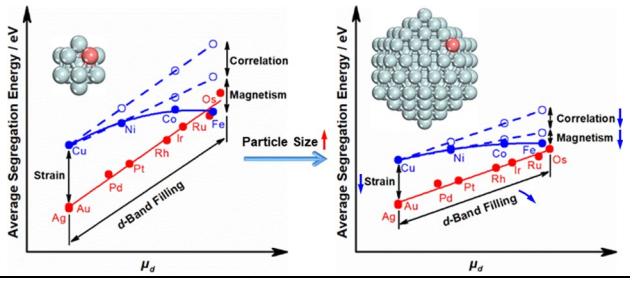
Average Segregation Energy / eV
Correlation
Magnetism
Particle Size
Strain
d-Band Filling
Cu
Ni
Co
Fe
Os
Ru
Ir
Rh
Pt
Pd
Au
Ag
μ_d